Geophysical Research Letters

RESEARCH LETTER
10.1029/2024GL110738

CMIP6 Models Underestimate ENSO Teleconnections in the Southern Hemisphere

Yingfei Fang[1], James A. Screen[2], Xiaoming Hu[1,3], Shuheng Lin[1], Ned C. Williams[4], and Song Yang[1,3]

[1]School of Atmospheric Sciences, Southern Marine Science and Engineering Guangdong Laboratory (Zhuhai), Sun Yat-sen University, Zhuhai, China, [2]Department of Mathematics and Statistics, University of Exeter, Exeter, UK, [3]Guangdong Province Key Laboratory for Climate Change and Natural Disaster Studies, Zhuhai, China, [4]Max-Planck-Institute for Meteorology, Hamburg, Germany

Key Points:

- CMIP6 models underestimate the intensity of observed ENSO teleconnection to the Amundsen Sea and simulate a westward bias in the wave train
- Experiments prescribed with historical global SST and sea ice, closely match the location and strength of observed ENSO-related wave train
- Increased ocean resolution eliminates the westward bias in the wave train responses to ENSO, but not their insufficient amplitudes

Supporting Information:

Supporting Information may be found in the online version of this article.

Correspondence to:

S. Yang and X. Hu,
yangsong3@mail.sysu.edu.cn;
huxm6@mail.sysu.edu.cn

Citation:

Fang, Y., Screen, J. A., Hu, X., Lin, S., Williams, N. C., & Yang, S. (2024). CMIP6 models underestimate ENSO teleconnections in the Southern Hemisphere. *Geophysical Research Letters*, *51*, e2024GL110738. https://doi.org/10.1029/2024GL110738

Received 9 JUN 2024
Accepted 6 SEP 2024

Author Contributions:

Conceptualization: Yingfei Fang, James A. Screen, Xiaoming Hu
Data curation: Ned C. Williams
Investigation: Yingfei Fang, Ned C. Williams
Methodology: Yingfei Fang, James A. Screen, Xiaoming Hu, Shuheng Lin, Ned C. Williams
Resources: Yingfei Fang
Software: Yingfei Fang
Supervision: Xiaoming Hu
Validation: Yingfei Fang
Visualization: Yingfei Fang, Shuheng Lin
Writing – original draft: Yingfei Fang

Abstract This study evaluates the capability of the Coupled Model Intercomparison Project Phase 6 (CMIP6) models to simulate El Niño-Southern Oscillation teleconnections in the Southern Hemisphere during austral summer. The wave trains from the tropical Pacific to the Amundsen Sea are underestimated and too far westward in CMIP6 simulations. However, Atmospheric Model Intercomparison Project Phase 6 (AMIP6) experiments well capture the observed location and amplitude of the teleconnection. El Niño and La Niña-related tropical precipitation anomalies are underestimated in CMIP6 and have their maximum amplitude too far westward, while the precipitation responses in AMIP6 simulations are similar to those observed. The weaker precipitation response in CMIP6 likely arises from a cold bias in climatological-mean SST, which reduces the sensitivity of precipitation to SST anomalies. Increased resolution in coupled experiments eradicates the westward bias in the El Niño and La Niña-related circulation anomalies over the Amundsen Sea, but not their insufficient amplitude.

Plain Language Summary Abnormally warm and cold sea surface temperatures (SST) in the tropical Pacific during El Niño and La Niña events, respectively, generate atmospheric circulation anomalies that propagate across the Southern Hemisphere toward the Amundsen Sea, where they influence west Antarctic climate. In this study, we evaluate how well state-of-the-art climate models simulate these El Niño and La Niña-related teleconnections. We find that free-running models simulate teleconnections that are too weak and too far westward. When models are provided with realistic SST however, they well simulate the teleconnection location and amplitude. The errors in free-running models likely occur because the models are too cold in the tropical Pacific, and this reduces the sensitivity of simulated rainfall to SST anomalies; and the SST anomalies are too far westward. Increased ocean resolution eradicates the error in the location of the El Niño and La Niña teleconnections but does not substantially improve their strength.

1. Introduction

The El Niño–Southern Oscillation (ENSO) is one of the dominant modes of tropical coupled atmosphere-ocean variability on interannual time scales (Wang & Fiedler, 2007), influencing global climate (Cai et al., 2011; DeConto & Pollard, 2016; Li et al., 2021; Yang et al., 2024; Yuan et al., 2020). ENSO-related anomalous convective heating generates stationary Rossby wave trains curving poleward and eastward toward Antarctica (Ciasto et al., 2015; Ding et al., 2012; Dong et al., 2023; Simpkins et al., 2016; Turner et al., 2013). During El Niño, the wave train from tropical Pacific induces an anomalous high-pressure center over the Amundsen Sea, which weakens the Amundsen Sea Low (ASL) (Chen et al., 2022; Ding et al., 2011; Li et al., 2015; Raphael et al., 2016; Turner et al., 2013). This leads to northerly and southerly wind anomalies to the west and east of the anomalous high-pressure, respectively, causing anomalous warm and cold advection (Gushchina et al., 2022; Scott et al., 2019), which increases sea ice in the Bellingshausen Sea and decreases sea ice in the Ross Sea (Isaacs et al., 2021; Wang et al., 2023). The associated anomalous circulation also exerts a non-negligible impact on ice shelf thinning through surface and basal melt (Huguenin et al., 2024; Li et al., 2023; Nicolas et al., 2017; Paolo et al., 2018).

The teleconnection patterns triggered by ENSO are sensitive to the location and amplitude of tropical sea surface temperature (SST) and precipitation anomalies, through their influences on convective heating. Eastern Pacific ENSO events often co-occur with the Indian Ocean Dipole, affecting a broader area across the Ross-Amundsen

Writing – review & editing: Yingfei Fang, James A. Screen, Xiaoming Hu, Shuheng Lin

and Bellingshausen-Weddell Seas, whereas the central Pacific ENSO has a more limited and localized impact (Guo et al., 2022; Zhang et al., 2021). Additionally, background flow patterns, particularly the subtropical jet, and transient eddy feedback also contribute to the differences in the geopotential height response in the mid-to-high latitudes (Beverley et al., 2021; Gillett et al., 2023; Kosaka & Nakamura, 2006; Wang et al., 2022a). The subtropical jet can support the development of an effective Rossby wave source, and the shift in the jet exit tends to alter the ENSO-related teleconnection pattern in the Southern Hemisphere, particularly during austral winter (Gillett et al., 2023; Sardeshmukh & Hoskin, 1988; Simmons et al., 1983; Wang et al., 2022b). The strength of the ENSO teleconnection to the Amundsen Sea region increases linearly with El Niño amplitude until it reaches its peak (Yiu & Maycock, 2020). However, there appear some systematic biases relevant to ENSO and the generation and propagation of its teleconnection in current models. The cold bias in mean-state SST in the eastern Pacific "cold tongue" and the excessive westward extension of SST anomalies has been discussed previously (Jiang et al., 2021; Li & Xie, 2014; Li et al., 2019). This cold bias contributes to an underestimation of tropical precipitation response to ENSO-related SST anomalies (Lin et al., 2024; Wang et al., 2021; Williams et al., 2024). Previous studies suggest that the underestimation of precipitation sensitivity to local SST and the error in modeling extratropical progresses may lead to underestimated ENSO teleconnections in the Northern Hemisphere (Good et al., 2021; Hardiman et al., 2022; Williams et al., 2023).

Here, we investigate the performance of coupled climate models from Coupled Model Intercomparison Project Phase 6 (CMIP6) in simulating ENSO teleconnections in the Southern Hemisphere and attempt to understand the biases (Eyring et al., 2016). We focus on austral summer due to the significant impact of ENSO on the West Antarctic climate, particularly, ice shelf surface melt, which predominantly occurs during summer in the current climate (Fang et al., 2024; Nicolas et al., 2017; Wang et al., 2023). However, for completeness, we include some analysis of the other seasons. Given the important role of the ASL on Antarctic climate, the reliability of climate models to simulate the influence of ENSO on the ASL is a primary focus of this study.

2. Data and Methods

We analyze the monthly outputs from the historical experiments of 60 CMIP6 models for the period of 1850–2014, and Atmospheric Model Intercomparison Project Phase 6 (AMIP6) experiments from 46 models for the period of 1979–2014 (refer to Tables S1 and S2 in Supporting Information S1). Additionally, we use hist-1950 simulations from 9 models with high oceanic resolution (HR; 0.25° or finer) and medium-to-high atmospheric resolution (139 km or finer) from the High Resolution Model Intercomparison Project (HighResMIP) for the period of 1950–2014 (Haarsma et al., 2016) (Table S3 in Supporting Information S1). For consistency, all model data sets are horizontally interpolated onto the same 2.5° × 2.5° grid using a bilinear interpolation method. We use all available ensemble members of each model, where the members within a model differ only in their initial conditions. This allows us to explore both the influence of internal variability (spread between members from a given model) and model uncertainty (spread between ensemble-means of different models). The uncertainty in the multi-model ensemble mean (MEM) is represented by calculating the standard error of the ensemble-means for each model, scaled by 1.96 to capture a 95% confidence interval.

This study analyzes reanalysis and observational data sets for the period of 1979–2023 as a reference. The data sets used include (a) SST data from the Hadley Centre Sea Ice and Sea Surface Temperature (HadISST), version 1 (Rayner et al., 2003); (b) precipitation data from the Global Precipitation Climatology Project (GPCP) (Adler et al., 2003); and (c) winds and geopotential height from fifth generation European Centre for Medium-range Weather Forecasts (ECMWF) atmospheric reanalysis (ERA5) released by the ECMWF (Hersbach et al., 2019).

We use standardized Niño3.4 index, which averages SST anomalies over 170°W–120°W, 5°S–5°N, to measure the ENSO intensity, and the index is calculated separately for observations and each model simulation. El Niño and La Niña events are defined based on thresholds of 1 and −1 standard deviation, respectively. Given that the peak phase of ENSO occurs during austral summer (December–February, inclusive; DJF), we focus on this season. We note that although we use the longest possible time period for the models, 1850–2014, to get better sampling of El Niño and La Niña events, our main results are also consistent if we sampled the models over the same time period as the observations (not shown).

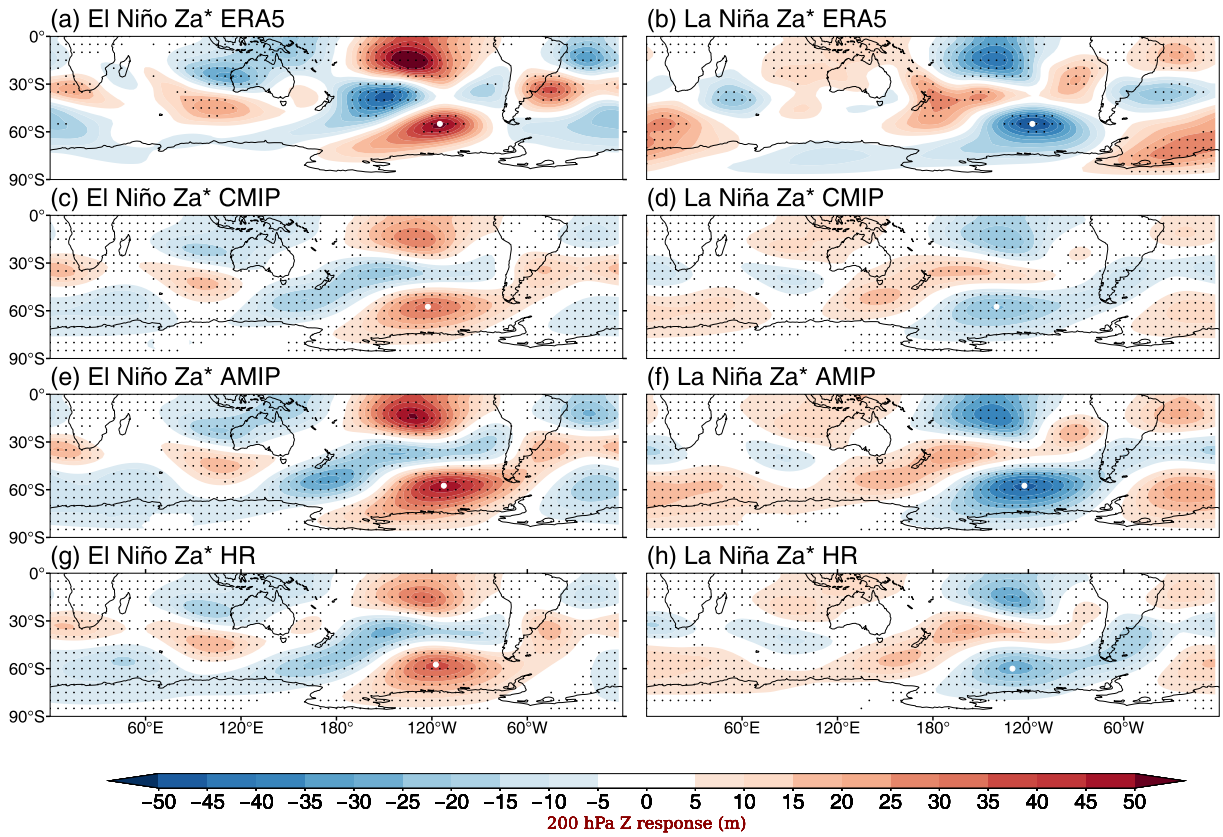

Figure 1. Composite patterns of DJF 200-hPa geopotential height anomalies in El Niño and La Niña in ERA5 (a, b), CMIP6 MEM (c, d), AMIP6 MEM (e, f), and HR MEM (g, h). White dot marks the center of geopotential height response in the Amundsen Sea region. The * in the subtitle indicates that the zonal mean of geopotential height has been subtracted. Stippling in all panels indicates that the composite result is above the 95% confidence level, with more than 70% of models agreeing on the sign of the MEM in (c)–(h).

3. Simulated ENSO Teleconnections

Figure 1 shows the composite-mean pattern of 200-hPa geopotential height anomalies during El Niño and La Niña in ERA5 and CMIP6 MEM. During El Niño, the anomalous tropical heating induces a Rossby wave train with a positive center located over the central tropical Pacific, a negative node over western South Pacific, and a second positive over the Amundsen Sea (Figure 1a). The pattern is reversed during La Niña (Figure 1b). The CMIP6 MEM shows broadly similar wave train patterns, but their amplitude is notably weaker than ERA5, for both El Niño and La Niña (Figures 1c and 1d). Similar results are also found for austral winter (Figure S1 in Supporting Information S1). The anomalous geopotential height center over the Amundsen Sea, important for west Antarctic climate, is simulated too far westward, again in both El Niño and La Niña. AMIP6 experiments prescribed with observed global SST and sea ice show wave train responses that are very similar to observations in both their location and amplitude (Figures 1e and 1f).

We further quantify the position and magnitude of the geopotential height anomaly center in the Amundsen Sea region (45°–90°S, 60°–180°W; Figure 2). Although there is substantial variation between members of a single model and between model ensemble means, significant common biases are evident. The amplitude of Amundsen Sea anomaly center during El Niño is 48 m in ERA5 but 32 m in the CMIP6 MEM. Although the CMIP6 MEM is within the range of observational uncertainty (Table 1), due to relatively poor sampling of observed El Niño events, it is striking that most members and models simulate weaker anomalies than observed, which is highly unlikely by chance (Figure 2a). During La Niña, the geopotential height response in the CMIP6 MEM is significantly weaker than ERA5 (−51 and −25 m, respectively; Table 1), and all models and nearly all members underestimate the anomaly center amplitude (Figure 2a). Similar underestimation is found in the other three seasons (Figure S2 in Supporting Information S1).

10.1029/2024GL110738

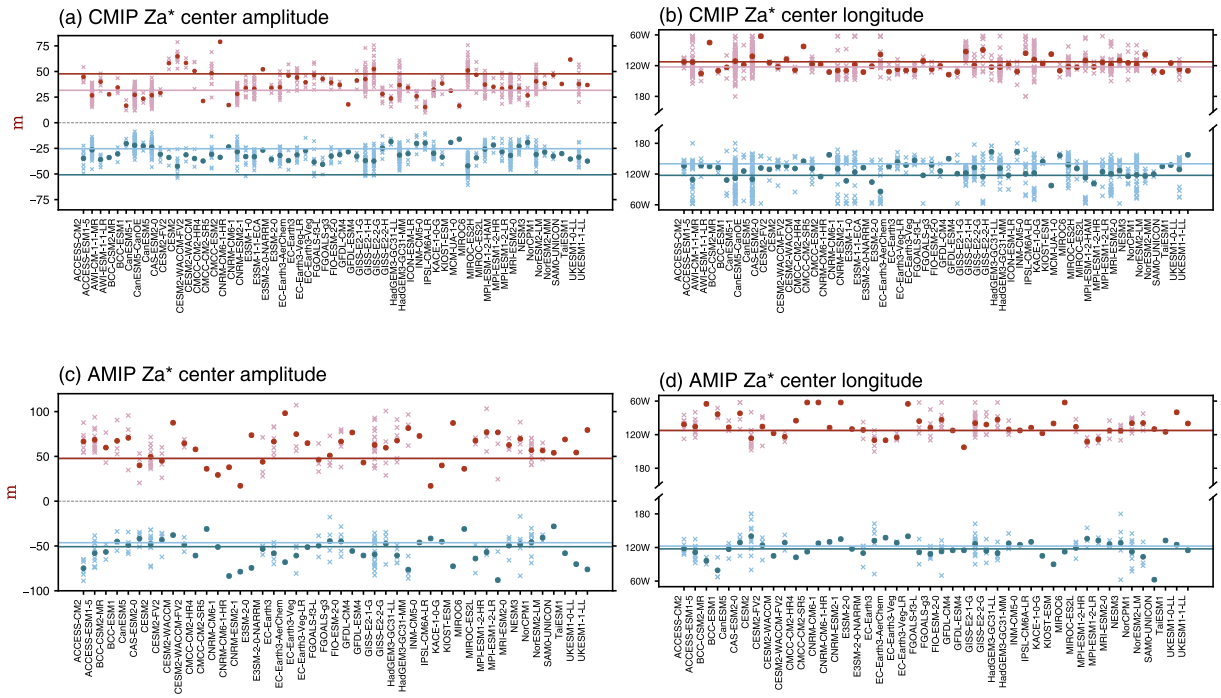

Figure 2. Magnitude and longitude of maximum geopotential height anomaly within 45°–90°S, 60°–180°W in CMIP6 (a, b) and AMIP6 (c, d). Red and blue crosses refer to El Niño and La Niña, respectively, for each member in each model, and red and blue dots represent the ensemble means for each model. Thin red and blue horizontal lines indicate the MEM for El Niño and La Niña, respectively, and thick red and blue lines show corresponding values from ERA5.

For the longitude of anomaly center, CMIP6 models tend to simulate a more westward location (Figure 2b), with a displacement of approximately 10° in El Niño and a notably significant 23° in La Niña compared to ERA5 (Table 1). The simulated westward bias of the Amundsen Sea anomaly center is present in most seasons and ENSO phases, except during El Niño in winter and La Niña in autumn. However, it is only statistically significant for La Niña in austral summer (Figure S2 in Supporting Information S1).

The AMIP6 MEM, however, closely matches ERA5 in both the longitude and amplitude of the anomaly center (Table 1). This indicates that when prescribed with historical global SST and sea ice, atmospheric models well reproduce the ENSO teleconnection to the Amundsen Sea. The geopotential height response in the high latitudes is relatively quasi-barotropic, with the structure at 500 hPa being similar to that at 200 hPa (Figure S3 in Supporting Information S1). The weaker amplitude of the Amundsen anomaly center in CMIP6 compared to ERA5 is evident throughout the troposphere for both El Niño and La Niña. At all tropospheric levels, AMIP6 is closer to ERA5 (albeit still weaker) than CMIP6 (Figure S4 in Supporting Information S1).

Table 1
Magnitude and Longitude of the Maximum Geopotential Height Anomaly Within 45°–90°S, 60°–180°W, the Niño3.4 Index, and Maximum Tropical Precipitation (Zonal Maximum of Meridional Mean Between 150°E and 140°W for 5°S–5°N), Along With Their 95% Confidence Intervals

	Amplitude (m)		Longitude (W)		Niño3.4 index (°C)		Max precipitation (mm/day)	
	El Niño	La Niña	El Niño	La Niña	El Niño	La Niña	El Niño	La Niña
ERA5/HadiSST/GPCP	47.7 ± 20.6	−50.8 ± 18.4	112.5 ± 24.4	117.5 ± 13.2	1.7 ± 0.4	−1.5 ± 0.2	6.9 ± 1.4	−4.1 ± 0.9
CMIP6	31.6 ± 3.1	**−25.3 ± 1.6**	122.5 ± 3.8	**140.0 ± 4.0**	1.7 ± 0.1	−1.6 ± 0.1	4.6 ± 0.4	−3.6 ± 0.3
AMIP6	47.9 ± 5.1	−46.3 ± 4.0	112.5 ± 5.8	122.5 ± 4.4	1.7 ± 0.4	−1.5 ± 0.2	6.7 ± 0.3	−5.0 ± 0.3
HR	38.0 ± 9.2	**−27.8 ± 4.7**	117.5 ± 7.1	127.5 ± 11.4	1.5 ± 0.2	−1.4 ± 0.2	5.2 ± 0.7	−4.0 ± 0.6

Note. Simulated values that are significantly different to ERA5 are shown in bold font. The Niño3.4 index in AMIP6 are derived from HadISST.

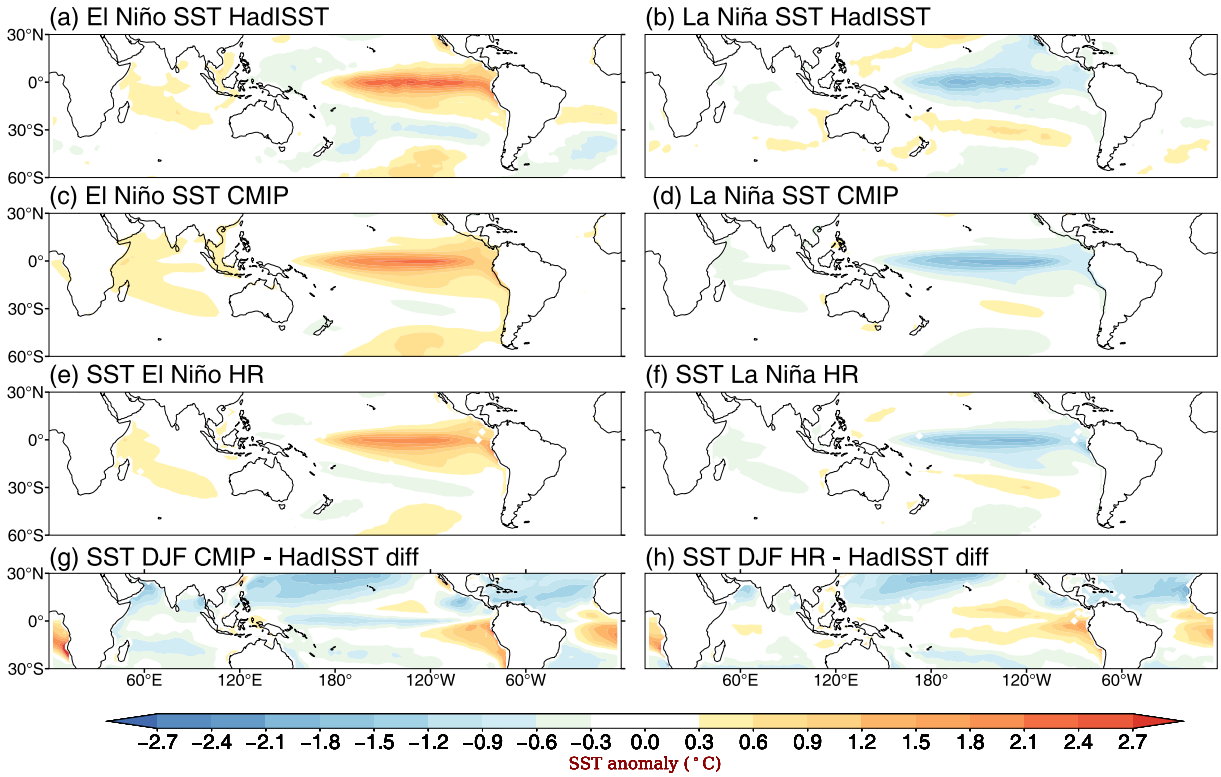

Figure 3. SST anomalies during El Niño and La Niña in observations (a, b), CMIP6 MEM (c, d), and HR MEM (e, f). Tropical climatological SST biases relative to observations in CMIP6 (g) and HR models (h).

4. Model SST Biases and Precipitation Sensitivity

The primary distinction between CMIP6 and AMIP6 is that the CMIP6 experiments simulate the interaction between atmosphere and ocean and therefore, exhibit SST biases, whereas the AMIP6 experiments are atmospheric models prescribed with historical ocean surface boundary conditions and therefore, by design, have realistic SST. Figure 3 shows the magnitude of SST anomalies in the tropical Pacific in the CMIP6 MEM is similar to that observed, but the simulated SST anomalies exhibit a westward extension in both El Niño and La Niña. Thus, the westward bias in the position of the Amundsen Sea anomaly center is likely related to the westward extension of the SST anomalies that determine the location of tropical heating and forcing of anomalous Rossby wave activity.

Strong convective activity and heavy rainfall in the tropics release latent heat and serve as an important forcing which triggers wave trains toward Antarctica. Figure 4 shows the positive precipitation and divergent wind responses during El Niño are significantly weaker than observed, even though the magnitudes of ENSO SST anomalies are realistic in CMIP6 (Table 1). Also, the tropical precipitation anomalies extend too far westward (Figure 4c), consistent with the westward extension of SST anomalies (Figure 3c). The maximum El Niño-related precipitation anomaly in GPCP is 6.9 mm/day, while in CMIP6, it is 4.6 mm/day. In contrast, in AMIP6, the maximum precipitation is 6.7 mm/day, and divergent wind anomalies are not significantly different from those in GPCP, which helps explain why the teleconnection amplitude is also better simulated in AMIP6 than in CMIP6. The Rossby wave source, which arises from the interaction between divergence and vorticity (the key factors in generating Rossby waves), is found to be underestimated in both tropics and subtropics in the CMIP6 models, while the AMIP6 simulations perform better (Figure S5 in Supporting Information S1). Similar results are found for La Niña, with CMIP6 models showing weaker and overly westward equatorial dry anomalies, compared to GPCP, whereas the AMIP6 simulations produce more realistic anomalies.

Previous studies reveal that the sensitivity of convection to a unit SST change increases monotonically with increasing mean state SST until it reaches a peak at approximately 28–29°C, after which it declines (Johnson & Xie, 2010; Lin et al., 2022; Waliser & Graham, 1993; Xie et al., 2020). Thus, even with the similar magnitude of

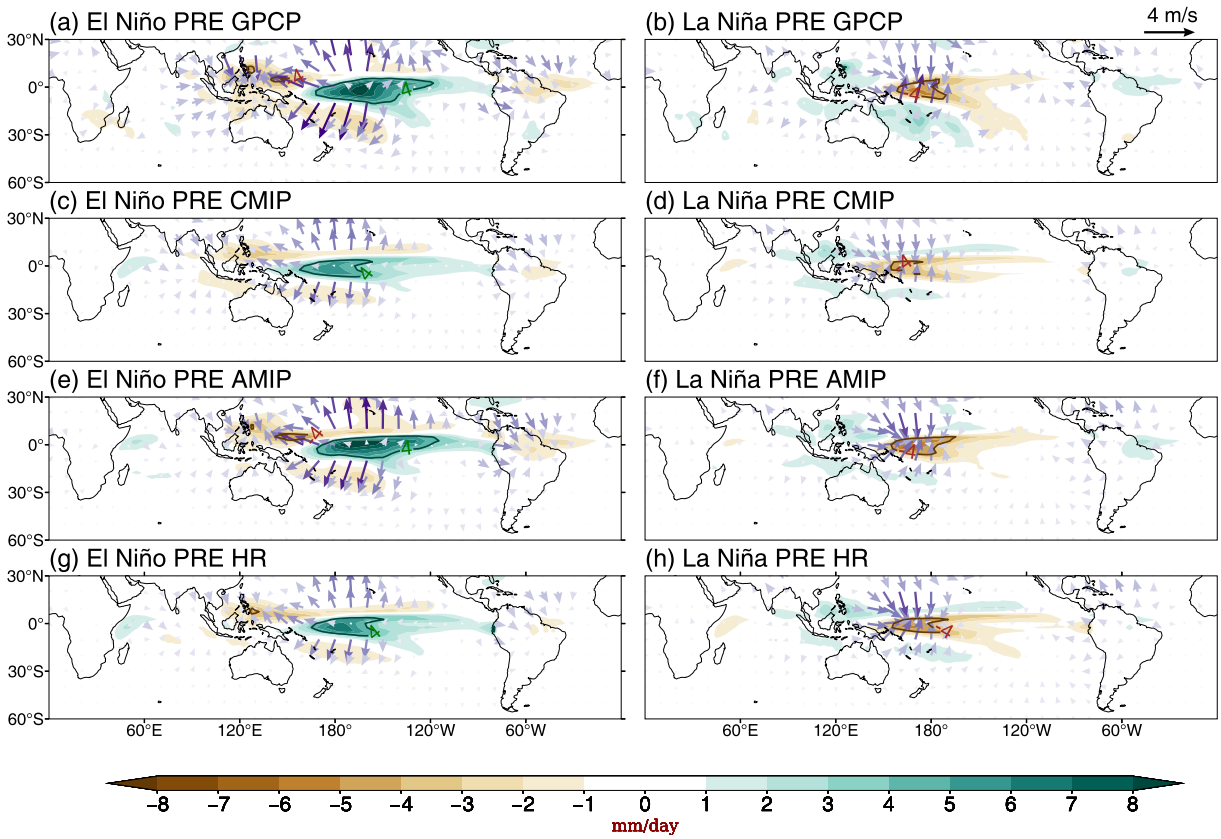

Figure 4. Composite patterns of precipitation and divergent wind anomalies during El Niño and La Niña in GPCP (a, b), CMIP6 MEM (c, d), AMIP6 MEM (e, f), and HR MEM (g, h). The shading of the vectors represents the magnitude of the values.

SST anomalies, the resulting precipitation anomalies can vary substantially between models and observations (and between different models). Figure 3g shows a 1°C cold bias of climatological-mean SST in the CMIP6 models, which suggests that the tropical precipitation sensitivity to SST is underestimated and helps to explain their too weak precipitation response to ENSO (Figure 4). Since the sensitivity of convection to SST increases with temperature before reaching its peak, the CMIP6 error in precipitation response is more pronounced during El Niño years, when SST is increased, compared to La Niña years when SST is decreased (Table 1).

5. Improvements at High Resolution

The results so far suggest that improved simulation of the mean state SST in coupled models may improve the accuracy of ENSO teleconnections. Liu et al. (2022) use the HighResMIP and find that increasing ocean resolution helps to improve the SST mean state in equatorial Pacific. Williams et al. (2024) show that bias of the westward extension of SST anomalies in the tropics during El Niño and La Niña is largely eliminated at higher ocean resolution, resulting in a more realistic location of the ENSO teleconnection to the Aleutian Low. Here, using the same simulations as Williams et al. (2024), we find a considerable improvement in the location of the geopotential height anomaly center in the Amundsen Sea, in HR compared to CMIP6 (Table 1), which we relate to the improved simulation of the westward extent of SST and precipitation anomalies in HR compared to CMIP6 (Figures 3 and 4). The CMIP6 and HR models differ in their atmospheric and oceanic resolution; however, Williams et al. (2024) demonstrated that it is increased oceanic resolution that leads to the improvements in HR.

The amplitude of the Amundsen Sea anomaly center is slightly higher in HR than CMIP6, but not significantly different, for El Niño or La Niña (Table 1). For La Niña, the amplitude remains significantly underestimated compared to ERA5. Thus, increased resolution does not resolve the overly weak ENSO teleconnection to the Amundsen Sea, consistent with Williams et al. (2024) results for the ENSO teleconnection to the Aleutian Low.

During El Niño, the maximum tropical Pacific precipitation anomaly is significantly increased in HR compared to CMIP6, albeit still less than observed. During La Niña, the precipitation anomaly in HR models is also of greater magnitude than CMIP6 and within observational uncertainty. Given the stronger precipitation anomalies in HR than CMIP6, it is perhaps surprising that the amplitude of the teleconnection is not appreciably improved. This is especially true for La Niña, when HR shows stronger than observed precipitation anomalies but a significantly too weak anomaly center over the Amundsen Sea. This suggests that model errors in the teleconnection strength may not solely relate to tropical biases, but also problems in the extratropics that influence wave propagation, consistent with Williams et al. (2023) for the ENSO teleconnection in the Northern Hemisphere. The realistic simulation of teleconnection strength in AMIP6 may provide some clues in this regard. Prescribing observed SST not only results in better ENSO-related SST and precipitation anomalies, but also reduces biases in the background circulation (Priestley et al., 2023), which may lead to improved ENSO teleconnections. Therefore, the weak teleconnections in CMIP6 and HR may partly arise due to errors in the circulation mean state, which are reduced in AMIP6. Previous studies have mentioned that the subtropical jet and eddy feedback could affect both the position and intensity of ENSO teleconnections (Gillett et al., 2023; Wang et al., 2022a, 2022b). However, the subtropical jet is absent during austral summer (Figure S6 in Supporting Information S1) in ERA5, CMIP6, and AMIP6, and therefore cannot affect the position and intensity of ENSO teleconnections or account for the weak teleconnection amplitude in CMIP6. Barotropic energy conversion in the subtropical Pacific (i.e., the conversion of local kinetic energy from the basic state to perturbations) is weaker in CMIP6 compared to ERA5 (Figure S7 in Supporting Information S1), which may partly explain the weaker teleconnection in CMIP6. The AMIP6 models simulate greater barotropic energy conversion (Figure S7 in Supporting Information S1), which could be one reason for their stronger ENSO teleconnections compared to CMIP6.

6. Conclusions

During ENSO events, anomalous SST in the tropical Pacific can trigger wave trains propagating from the tropics to the Amundsen Sea, influencing climate over West Antarctica. This study investigates the capability of the CMIP6 models to reproduce this teleconnection and reveals that the models generally underestimate its intensity and place it too far westward, in El Niño and especially La Niña. In contrast, AMIP6 experiments, prescribed with historical global SST and sea ice, accurately reproduce the location and amplitude of the teleconnections.

The biases in teleconnections in the CMIP6 models stem from the underestimation and too far westward extension of ENSO-related precipitation anomalies. This underestimation occurs despite realistic magnitudes of ENSO-related SST anomalies and is explained by a cold bias in the mean-state SST in the CMIP6 models, which reduces the sensitivity of precipitation to SST anomalies. In AMIP6, absent mean-state SST biases, the position and intensity of precipitation anomalies are accurately simulated and thus, so is the location and the strength of the wave train to the Amundsen Sea.

Increased oceanic resolution leads to improvement in simulating the SST mean state and westward extent of ENSO-related SST anomalies, and consequently enhances the accuracy of anomalous precipitation and the location of the teleconnection to the Amundsen Sea. However, even at high resolution, coupled models still underestimate the intensity of the Amundsen Sea anomaly center, particularly during La Niña, despite accurately simulating the amplitude of ENSO-related precipitation anomalies that drive the wave train. Further work is needed to better understand model biases in the propagation of the ENSO teleconnections from the tropics to the extratropics.

Data Availability Statement

The HadISST data set is downloaded from the UK Met Office at https://www.metoffice.gov.uk/hadobs/hadisst/data/download.html. The ERA5 monthly reanalysis data can be downloaded from Hersbach et al. (2023). The GPCP monthly precipitation data is downloaded from https://psl.noaa.gov/data/gridded/data.gpcp.html. The CMIP6 and AMIP6 models used in this study are listed in Tables S1–S3 of the Supporting Information S1, and their output are available at https://esgf-node.llnl.gov/search/CMIP6/.

Acknowledgments
The authors thank the editor Dr. Gudrun Magnusdottir and two anonymous reviewers for their valuable comments which helped greatly to improve the manuscript. This study was jointly supported by the National Natural Science Foundation of China (Grant 42075028), the Southern Marine Science and Engineering Guangdong Laboratory (Zhuhai) (Grants 316323005 and SML2021SP302), and the Science and Technology Planning Project of Guangdong Province (2023B1212060019)

References

Adler, R. F., Huffman, G. J., Chang, A., Ferraro, R., Xie, P. P., Janowiak, J., et al. (2003). The version-2 global precipitation climatology project (GPCP) monthly precipitation analysis (1979-present). *Journal of Hydrometeorology*, *4*(6), 1147–1167. https://doi.org/10.1175/1525-7541(2003)004<1147:TVGPCP>2.0.CO;2

Beverley, J. D., Collins, M., Lambert, F. H., & Chadwick, R. (2021). Future changes to El Niño teleconnections over the North Pacific and North America. *Journal of Climate*, *34*(15), 6191–6205. https://doi.org/10.1175/JCLI-D-20-0877.1

Cai, W., Rensch, P. V., Cowan, T., & Hendon, H. H. (2011). Teleconnection pathways of ENSO and the IOD and the mechanisms for impacts on Australian rainfall. *Journal of Climate*, *24*(15), 3910–3923. https://doi.org/10.1175/2011JCLI4129.1

Chen, J., Hu, X., Yang, S., Lin, S., & Li, Z. (2022). Influence of convective heating over the Maritime Continent on the West Antarctic climate. *Geophysical Research Letters*, *49*(9), 1–10. https://doi.org/10.1029/2021GL097322

Ciasto, L. M., Simpkins, G. R., & England, M. H. (2015). Teleconnections between tropical Pacific SST anomalies and extratropical Southern Hemisphere climate. *Journal of Climate*, *28*(1), 56–65. https://doi.org/10.1175/JCLI-D-14-00438.1

DeConto, R. M., & Pollard, D. (2016). Contribution of Antarctica to past and future sea-level rise. *Nature*, *531*(7596), 591–597. https://doi.org/10.1038/nature17145

Ding, Q., Steig, E. J., Battisti, D. S., & Küttel, M. (2011). Winter warming in West Antarctica caused by central tropical Pacific warming. *Nature Geoscience*, *4*(6), 398–403. https://doi.org/10.1038/ngeo1129

Ding, Q., Steig, E. J., Battisti, D. S., & Wallace, J. M. (2012). Influence of the tropics on the southern annular mode. *Journal of Climate*, *25*(18), 6330–6348. https://doi.org/10.1175/JCLI-D-11-00523.1

Dong, C., Peings, Y., & Magnusdottir, G. (2023). Regulation of southwestern United States precipitation by non-ENSO teleconnections and the impact of the background flow. *Journal of Climate*, *36*(21), 7415–7433. https://doi.org/10.1175/JCLI-D-23-0081.1

Eyring, V., Bony, S., Meehl, G. A., Senior, C. A., Stevens, B., Stouffer, R. J., & Taylor, K. E. (2016). Overview of the Coupled Model Intercomparison Project Phase 6 (CMIP6) experimental design and organization. *Geoscientific Model Development*, *9*(5), 1937–1958. https://doi.org/10.5194/gmd-9-1937-2016

Fang, Y., Yang, S., Hu, X., Lin, S., Screen, J. A., & Chen, S. (2024). Remote forcing for circulation pattern favorable to surface melt over the Ross Ice Shelf. *Journal of Climate*, 1–31. https://doi.org/10.1175/jcli-d-23-0120.1

Gillett, Z. E., Hendon, H. H., Arblaster, J. M., & Lin, H. (2023). Sensitivity of the Southern Hemisphere wintertime teleconnection to the location of ENSO heating. *Journal of Climate*, *36*(8), 2497–2514. https://doi.org/10.1175/JCLI-D-22-0159.1

Good, P., Chadwick, R., Holloway, C. E., Kennedy, J., Lowe, J. A., Roehrig, R., & Rushley, S. S. (2021). High sensitivity of tropical precipitation to local sea surface temperature. *Nature*, *589*(7842), 408–414. https://doi.org/10.1038/s41586-020-2887-3

Guo, Y., Wen, Z., Zhu, Y., & Chen, X. (2022). Effect of the late-1990s change in tropical forcing on teleconnections to the Amundsen-Bellingshausen seas region during austral autumn. *Journal of Climate*, *35*(17), 5687–5702. https://doi.org/10.1175/JCLI-D-21-0965.1

Gushchina, D., Kolennikova, M., Dewitte, B., & Yeh, S. W. (2022). On the relationship between ENSO diversity and the ENSO atmospheric teleconnection to high-latitudes. *International Journal of Climatology*, *42*(2), 1303–1325. https://doi.org/10.1002/joc.7304

Haarsma, R. J., Roberts, M. J., Vidale, P. L., Catherine, A., Bellucci, A., Bao, Q., et al. (2016). High resolution model intercomparison project (HighResMIP v1.0) for CMIP6. *Geoscientific Model Development*, *9*(11), 4185–4208. https://doi.org/10.5194/gmd-9-4185-2016

Hardiman, S. C., Dunstone, N. J., Scaife, A. A., Smith, D. M., Comer, R., Nie, Y., & Ren, H. L. (2022). Missing eddy feedback may explain weak signal-to-noise ratios in climate predictions. *Npj Climate and Atmospheric Science*, *5*(1), 1–8. https://doi.org/10.1038/s41612-022-00280-4

Hersbach, H., Bell, B., Berrisford, P., Biavati, G., Horányi, A., Muñoz Sabater, J., et al. (2023). ERA5 monthly averaged data on pressure levels from 1940 to present [Dataset]. *Copernicus Climate Change Service (C3S) Climate Data Store (CDS)*. https://doi.org/10.24381/cds.6860a573

Hersbach, H., Bell, B., Berrisford, P., Horányi, A., Sabater, J. M., Nicolas, J., et al. (2019). Global reanalysis: Goodbye ERA-Interim, hello ERA5. *ECMWF Newsletter*, *159*, 17–24. https://doi.org/10.21957/vf291hehd7

Huguenin, M. F., Holmes, R. M., Spence, P., & England, M. H. (2024). Subsurface warming of the West Antarctic continental shelf linked to El Niño-Southern Oscillation. *Geophysical Research Letters*, *51*(7), e2023GL104518. https://doi.org/10.1029/2023GL104518

Isaacs, F. E., Renwick, J. A., Mackintosh, A. N., & Dadic, R. (2021). ENSO modulates summer and autumn sea ice variability around Dronning Maud Land, Antarctica. *Journal of Geophysical Research: Atmospheres*, *126*(5), 1–17. https://doi.org/10.1029/2020JD033140

Jiang, W., Huang, P., Huang, G., & Ying, J. (2021). Origins of the excessive westward extension of ENSO SST simulated in CMIP5 and CMIP6 models. *Journal of Climate*, *34*(8), 2839–2851. https://doi.org/10.1175/JCLI-D-20-0551.1

Johnson, N. C., & Xie, S. P. (2010). Changes in the sea surface temperature threshold for tropical convection. *Nature Geoscience*, *3*(12), 842–845. https://doi.org/10.1038/ngeo1008

Kosaka, Y., & Nakamura, H. (2006). Structure and dynamics of the summertime Pacific–Japan teleconnection pattern. *Quarterly Journal of the Royal Meteorological Society*, *132*(619), 2009–2030. https://doi.org/10.1256/qj.05.204

Li, G., Jian, Y., Yang, S., Du, Y., Wang, Z., Li, Z., et al. (2019). Effect of excessive equatorial Pacific cold tongue bias on the El Niño-Northwest Pacific summer monsoon relationship in CMIP5 multi-model ensemble. *Climate Dynamics*, *52*(9–10), 6195–6212. https://doi.org/10.1007/s00382-018-4504-9

Li, G., & Xie, S. P. (2014). Tropical biases in CMIP5 multimodel ensemble: The excessive equatorial Pacific cold tongue and double ITCZ problems. *Journal of Climate*, *27*(4), 1765–1780. https://doi.org/10.1175/JCLI-D-13-00337.1

Li, W., Wu, Y., & Hu, X. (2023). The processes-based attributes of four major surface melting events over the Antarctic Ross Ice Shelf. *Advances in Atmospheric Sciences*, *40*, 1662–1670. https://doi.org/10.1007/s00376-023-2287-3

Li, X., Cai, W., Meehl, G. A., Chen, D., Yuan, X., Raphael, M., et al. (2021). Tropical teleconnection impacts on Antarctic climate changes. *Nature Reviews Earth & Environment*, *2*(10), 680–698. https://doi.org/10.1038/s43017-021-00204-5

Li, X., Gerber, E. P., Holland, D. M., & Yoo, C. (2015). A Rossby wave bridge from the tropical Atlantic to West Antarctica. *Journal of Climate*, *28*(6), 2256–2273. https://doi.org/10.1175/JCLI-D-14-00450.1

Lin, S., Dong, B., & Yang, S. (2024). Enhanced impacts of ENSO on the Southeast Asian summer monsoon under global warming and associated mechanisms. *Geophysical Research Letters*, *51*(2), e2023GL106437. https://doi.org/10.1029/2023GL106437

Lin, S., Yang, S., He, S., Li, Z., Chen, J., Dong, W., & Wu, J. (2022). Attribution of the seasonality of atmospheric heating changes over the western tropical Pacific with a focus on the spring season. *Climate Dynamics*, *58*(9–10), 2575–2592. https://doi.org/10.1007/s00382-021-06020-3

Liu, B., Gan, B., Cai, W., Wu, L., Geng, T., Wang, H., et al. (2022). Will increasing climate model resolution be beneficial for ENSO simulation? *Geophysical Research Letters*, *49*(11), 1–11. https://doi.org/10.1029/2021GL096932

Nicolas, J. P., Vogelmann, A. M., Scott, R. C., Wilson, A. B., Cadeddu, M. P., Bromwich, D. H., et al. (2017). 2016 extensive summer melt in West Antarctica favoured by strong El Niño. *Nature Communications*, *8*(15799), 15799. https://doi.org/10.1038/ncomms15799

Paolo, F. S., Padman, L., Fricker, H. A., Adusumilli, S., Howard, S., & Siegfried, M. R. (2018). Response of Pacific-sector Antarctic ice shelves to the El Niño/Southern Oscillation. *Nature Geoscience*, *11*(2), 121–126. https://doi.org/10.1038/s41561-017-0033-0

Priestley, M. D. K., Ackerley, D., Catto, J. L., & Hodges, K. I. (2023). Drivers of biases in the CMIP6 extratropical storm tracks. Part II: Southern Hemisphere. *Journal of Climate*, *36*(5), 1469–1486. https://doi.org/10.1175/JCLI-D-20-0977.1

Raphael, M. N., Marshall, G. J., Turner, J., Fogt, R. L., Schneider, D., Dixon, D. A., et al. (2016). The Amundsen Sea low: Variability, change, and impact on Antarctic climate. *Bulletin of the American Meteorological Society*, *97*(1), 111–121. https://doi.org/10.1175/BAMS-D-14-00018.1

Rayner, N. A., Parker, D. E., Horton, E. B., Folland, C. K., Alexander, L. V., Rowell, D. P., et al. (2003). Global analyses of sea surface temperature, sea ice, and night marine air temperature since the late nineteenth century. *Journal of Geophysical Research*, *108*(14), 4407. https://doi.org/10.1029/2002jd002670

Sardeshmukh, P. D., & Hoskin, B. J. (1988). The generation of global rotation flow by steady idealized tropical divergence. *Journal of the Atmospheric Sciences*, *45*(7), 1228–1251. https://doi.org/10.1175/1520-0469(1988)045%3C1228:TGOGRF%3E2.0.CO;2

Scott, R. C., Nicolas, J. P., Bromwich, D. H., Norris, J. R., & Lubin, D. (2019). Meteorological drivers and large-scale climate forcing of West Antarctic surface melt. *Journal of Climate*, *32*(3), 665–684. https://doi.org/10.1175/JCLI-D-18-0233.1

Simmons, A. J., Wallace, J. M., & Branstator, G. W. (1983). Barotropic wave propagation and instability, and atmospheric teleconnection Patterns. *Journal of the Atmospheric Sciences*, *40*(6), 1363–1392. https://doi.org/10.1175/1520-0469(1983)040<1363:BWPAIA>2.0.CO;2

Simpkins, G. R., Peings, Y., & Magnusdottir, G. (2016). Pacific influences on tropical Atlantic teleconnections to the Southern Hemisphere high latitudes. *Journal of Climate*, *29*(18), 6425–6444. https://doi.org/10.1175/JCLI-D-15-0645.1

Turner, J., Phillips, T., Hosking, J. S., Marshall, G. J., & Orr, A. (2013). The Amundsen Sea low. *International Journal of Climatology*, *33*(7), 1818–1829. https://doi.org/10.1002/joc.3558

Waliser, D. E., & Graham, N. E. (1993). Convective cloud systems and warm-pool sea surface temperatures: Coupled interactions and self-regulation. *Journal of Geophysical Research*, *98*(D7), 12881–12893. https://doi.org/10.1029/93jd00872

Wang, C., & Fiedler, P. C. (2007). Erratum to "ENSO variability and the eastern tropical Pacific: A review". *Progress in Oceanography*, *72*(4), 384. https://doi.org/10.1016/j.pocean.2006.11.001

Wang, J., Luo, H., Yu, L., Li, X., Holland, P. R., & Yang, Q. (2023). The impacts of combined SAM and ENSO on seasonal Antarctic sea ice changes. *Journal of Climate*, *36*(11), 3553–3569. https://doi.org/10.1175/JCLI-D-22-0679.1

Wang, X. Y., Zhu, J., Chang, C. H., Johnson, N. C., Liu, H., Li, Y., et al. (2021). Underestimated responses of Walker circulation to ENSO-related SST anomaly in atmospheric and coupled models. *Geoscience Letters*, *8*(1), 17. https://doi.org/10.1186/s40562-021-00186-8

Wang, Y., Huang, G., Hu, K., Tao, W., Gong, H., Yang, K., & Tang, H. (2022a). Understanding the eastward shift and intensification of the ENSO teleconnection over South Pacific and Antarctica under greenhouse warming. *Frontiers in Earth Science*, *10*, 1–9. https://doi.org/10.3389/feart.2022.916624

Wang, Y., Huang, G., Hu, K., Tao, W., Li, X., Gong, H., et al. (2022b). Asymmetric impacts of El Niño and La Niña on the Pacific–South America teleconnection pattern. *Journal of Climate*, *35*(6), 1825–1838. https://doi.org/10.1175/JCLI-D-21-0285.1

Williams, N. C., Scaife, A. A., & Screen, J. A. (2023). Underpredicted ENSO teleconnections in seasonal forecasts. *Geophysical Research Letters*, *50*(5), 1–9. https://doi.org/10.1029/2022GL101689

Williams, N. C., Scaife, A. A., & Screen, J. A. (2024). Effect of increased ocean resolution on model errors in El Niño–Southern Oscillation and its teleconnections. *Quarterly Journal of the Royal Meteorological Society*, *150*, 1489–1500. https://doi.org/10.1002/qj.4655

Xie, R., Mu, M., & Fang, X. (2020). New indices for better understanding ENSO by incorporating convection sensitivity to sea surface temperature. *Journal of Climate*, *33*(16), 7045–7061. https://doi.org/10.1175/JCLI-D-19-0239.1

Yang, S., Chen, D., & Deng, K. (2024). Global effects of climate change in the South China Sea and its surrounding areas. *Ocean-Land-Atmosphere Research*, *3*, 1–13. https://doi.org/10.34133/olar.0038

Yiu, Y. Y. S., & Maycock, A. C. (2020). The linearity of the El Niño teleconnection to the Amundsen Sea region. *Quarterly Journal of the Royal Meteorological Society*, *146*(728), 1169–1183. https://doi.org/10.1002/qj.3731

Yuan, S., Xu, J., Chan, J. C. L., Chiu, L. S., & Pan, Y. (2020). Resonance effect in interaction between South Asian summer monsoon and ENSO during 1958–2018. *Journal of Tropical Meteorology*, *26*(2), 137–149. https://doi.org/10.46267/j.1006-8775.2020.013

Zhang, C., Li, T., & Li, S. (2021). Impacts of CP and EP El Nino events on the Antarctic sea ice in austral spring. *Journal of Climate*, *34*(23), 9327–9348. https://doi.org/10.1175/JCLI-D-21-0002.1